



Slant Column Measurements of O₃ and NO₂ During the NDSC Intercomparison of Zenith-Sky UV-Visible Spectrometers in June 1996

H. K. ROSCOE¹, P. V. JOHNSTON², M. VAN ROOZENDAEL³, A. RICHTER⁴,
A. SARKISSIAN⁵, J. ROSCOE¹, K. E. PRESTON¹, J-C. LAMBERT³,
C. HERMANS³, W. DECUYPER³, S. DZIENUS⁴, T. WINTERRATH⁴,
J. BURROWS⁴, F. GOUTAIL⁵, J-P. POMMEREAU⁵, E. D'ALMEIDA⁵,
J. HOTTIER⁵, C. COUREUL⁵, R. DIDIER⁵, I. PUNDT⁵, L. M. BARTLETT⁶,
C. T. McELROY⁷, J. E. KERR⁷, A. ELOKHOV⁸, G. GIOVANELLI⁹,
F. RAVEGNANI⁹, M. PREMUDA⁹, I. KOSTADINOV⁹, F. ERLE¹⁰,
T. WAGNER¹⁰, K. PFEILSTICKER¹⁰, M. KENNTNER¹⁰, L. C. MARQUARD¹⁰,
M. GIL¹¹, O. PUENTEDURA¹¹, M. YELA¹¹, D. W. ARLANDER¹²,
B. A. KASTAD HOISKAR¹², C. W. TELLEFSEN¹²,
K. KARLSEN TORNKVIST¹², B. HEESE¹³, R. L. JONES¹⁴, S. R. ALIWELL¹⁴
and R. A. FRESHWATER¹⁴

¹British Antarctic Survey/NERC, Madingley Rd., Cambridge CB3 0ET, U.K.

²NIWA, PB 50061, Omakau, Central Otago, New Zealand

³IASB, 3 Ave. Circulaire, B-1180 Brussels, Belgium

⁴University of Bremen, PO Box 34404, Inst. Environmental Phys., D-28334 Bremen, Germany

⁵Service d'Aeronomie du CNRS, BP3, 91371 Verrieres le Buisson, France

⁶University of Wales, Physics Dept., Aberystwyth SY23 3BZ, U.K.

⁷AES, 4905 Dufferin Street, Downsview ON, Canada M3H 5T4

⁸Institute of Atmospheric Physics, Moscow, Russia

⁹CNR, Fisbat Institute, Via Gobetti 101, 40129 Bologna, Italy

¹⁰University of Heidelberg, Inst. Umweltphysik, INF 366, 69120 Heidelberg, Germany

¹¹INTA, Calle Ajalvir Km 4, 28850 Torrejon de Ardoz, Madrid, Spain

¹²NILU, PO Box 100, 2007 Kjeller, Norway

¹³UNIS, PO Box 156, N-9170 Longyearbyen, Norway

¹⁴Centre for Atmospheric Science, University of Cambridge, Department of Chemistry, Lensfield Road, Cambridge CB2 1EW, U.K.

(Received: 11 March 1998; accepted: 7 September 1998)

Abstract. In June 1996, 16 UV-visible sensors from 11 institutes measured spectra of the zenith sky for more than 10 days. Spectra were analysed in real-time to determine slant column amounts of O₃ and NO₂. Spectra of Hg lamps and lasers were measured, and the amount of NO₂ in a cell was determined by each spectrometer. Some spectra were re-analysed after obvious errors were found. Slant columns were compared in two ways: by examining regression analyses against comparison instruments over the whole range of solar zenith angles; and by taking fractional differences from a comparison instrument at solar zenith angles between 85° and 91°. Regression identified which pairs of instruments were most consistent, and so which could be used as universal comparison in-

struments. For O₃, regression slopes for the whole campaign agreed within 5% for most instruments despite the use of different cross-sections and wavelength intervals, whereas similar agreement was only achieved for NO₂ when the same cross-sections and wavelength intervals were used and only one half-day's data was analysed. Mean fractional differences in NO₂ from a comparison instrument fall within $\pm 7\%$ (1-sigma) for most instruments, with standard deviations of the mean differences averaging 4.5%. Mean differences in O₃ fall within $\pm 2.5\%$ (1-sigma) for most instruments, with standard deviations of the mean differences averaging 2%. Measurements of NO₂ in the cell had similar agreement to measurements of NO₂ in the atmosphere, but for some instruments measurements with cell and atmosphere relative to a comparison instrument disagreed by more than the error bars.

Key words: ozone, NO₂, UV-visible.

1. Introduction

Since their early use to measure NO₂ (Brewer *et al.*, 1973; Noxon, 1975), UV-visible spectrometers which observe the zenith sky provided the simplest method for routine observations of the total vertical column of O₃ and NO₂ from the ground. By observing sunlight scattered from the zenith sky, observations can be made in any weather. Modern detectors and control systems allow fully automated apparatus, and with no moving parts thereby enhancing their reliability. Detectors and spectrometers which operate at UV-visible wavelengths are lower-cost than those which operate at other wavelengths. For these reasons, there are now over 20 UV-visible spectrometers deployed world-wide, making continuous measurements. Some are primary instruments within the international Network for Determination of Stratospheric Change (NDSC), and many others are associated with NDSC as complementary instruments. The NDSC promotes excellence in stratospheric measurements. One part of ensuring accuracy of measurements is to compare instruments and analyses when measuring and analysing identical fields, and NDSC holds intercomparisons of instruments and analysis techniques from time to time. Measurements of slant columns of NO₂ by UV-visible zenith-sky spectrometers were compared in New Zealand in 1992 (Hofmann *et al.*, 1995), after which two instruments were fully certified for NDSC use with partial certification for others. In 1994 in the U.K., a selection European sensors of both O₃ and NO₂ were compared, under European Union (EU) sponsorship (Vaughan *et al.*, 1997). Vertical columns were deduced, with some O₃ results of comparable accuracy to Dobson measurements, and a recommendation was made of the best method to determine the amount in the reference spectrum (Sarkissian *et al.*, 1997).

Following these successes, the European consortium Stratospheric Climatology from UV-Visible Sensors (SCUVS) was awarded an EU contract which included a full intercomparison campaign of sensors of O₃ and NO₂ under NDSC auspices in 1996, which we discuss in this paper. It is an advance on the New-Zealand intercomparison because we also included sensors of O₃, and we determined NO₂ amounts from laboratory cross-sections without cell correction factors. It is an

advance on the U.K. intercomparison because we included a larger selection of instrument styles, and we focus on slant-column measurements which are at the heart of instrument quality. It is an advance on both intercomparisons because we devise a way to find which are the best sets of measurements when this is not known a priori (Section 4.1), and because we examine the value of measurements of a cell containing NO₂ as an intercomparison tool compared to measurements of NO₂ in the atmosphere (Section 5).

2. The Intercomparison Campaign

The campaign took place at the Observatoire de Haute Provence (OHP) in Southern France at 43.9° N, 5.7° E, in the NDSC Lidar complex, which also houses an automated Dobson and a UV-visible spectrometer of the design Systeme d'Analyse par Observations Zenithales (SAOZ) (Pommereau and Goutail, 1988). More than 40 scientists from 11 institutes participated in the campaign, bringing the 16 instruments described in Table I. Three weeks were allocated for the campaign. An initial few days of setting up was followed by ten days of intensive observations.

By common consent of the participants, the campaign started as single-blind, but gradually became open if participants had the time and energy to examine other data, not usually the case. Initially, slant columns were plotted without names and displayed for discussion at the next day's meeting. By inspecting the plots and knowing their own values, instrument representatives could tell if their values were very different to any consensus, but no other details. After about 5 days, the analysis task had become so intensive for those instruments which rarely used a daily reference spectrum (see below) that the plots were rarely inspected, so the referee (HKR) notified instrument representatives if there was an obvious error so that it could be corrected immediately. At the end of the formal campaign, plots of mean differences from one instrument were discussed, with instrument names on plots. After this time, revisions were only accepted where full details of the reasons for changes were supplied.

Most instruments measured slant columns on most days. There were some problems which led to loss of data, summarised in Table II. During the campaign, ambient temperatures usually fell below 15 °C by dawn and rose above 25 °C by noon, sometimes above 30 °C. These large diurnal temperature changes led to significant changes in wavelength calibrations in un-thermostated instruments, and the high afternoon temperatures led to some overheating in thermostated instruments. On some afternoons heavy cloud and thunderstorms combined with photochemical smog (clearly visible to the South earlier in the day), leading to elimination of those afternoons from the intercomparison, as discussed below. Radiosondes temperatures were consistent with a tropopause height near 12 km, but some ozonesondes had a secondary minimum in ozone at 16 km, consistent with some air at that altitude being transported from further South.

Table I. Specifications of spectrometers in the NDSC UV-visible intercomparison campaign in June 1996

Group and instrument	Spectral range (nm)	Grating		<i>f</i> -number	Detector		Number of pixels	Temp. stab. ^d	Fibre	Polariser	Resolution FWHM (nm)	Sampling ratio (pixel/FWHM)	FOV (degrees full angle)	Sky image on grating	Modifications for this campaign	References
		Type	Density (gr/mm)		Type	T (°C)										
Aber	289–611	c, h	200	2.9	NMOS	Ambient	512	no	no	no	0.9	1.8	20	yes	–	Pommereau and Goutail (1988)
AES7	426–456	p, h	1200	6.0	PMT	Ambient	–	no	no	film	1.0	– ^b	1.5	yes	–	Kerr <i>et al.</i> (1985)
AES22	431–454 ^a	p, h	1200	6.0	PMT	Ambient	–	no	no	film	1.0	3.3S/10R	1.5	yes	scanning	Kerr <i>et al.</i> (1985)
Brem	340–502	p, r	300	6.9	Ret	–35	1024	yes	bundle	no	1.3	8	1	no	–	Richter (1997)
CNR	408–464	c, h	1200	5.0	NMOS	–10/–25	512	no	no	film	0.6	5	≪1	no	–	Hofmann <i>et al.</i> (1995)
CNRS2, 3 and NILU2	277–634	c, h	360	2.9	NMOS	Ambient	1024	no	no	no	1.1	2.9	20	yes	–	Pommereau and Goutail (1988)
Heidv	374–690	c, h	1040		Ret	–35	1024	yes	bundle	no	1.8	6.2	1	no	–	Vaughan <i>et al.</i> (1997)
HeidU	300–404	c, h	819		Ret	–32	1024	yes	bundle	no	0.6	6	<1	no	–	Vaughan <i>et al.</i> (1997)
IASB	400–555	p, r	1200	3.7	Ret	–38	1024	yes	quartz	no	1.0	6	1	no	fibre	Vaughan <i>et al.</i> (1997)
INTA	335–639	p, r	600	3.8	Ret	–30	1024	yes	liquid	no	1.4	5	16	no	–	Gil <i>et al.</i> (1996)
NILU1	332–482	p, r	600	3.2	NMOS	–30	1024	yes	bundle	no	0.9	6.1	18	no	–	Karlsen <i>et al.</i> (1996)
NIWa	426–490	p, h	2400	5.0	PMT	33	–	yes	no	G-T	1.2	19	15	yes	polariser	Hofmann <i>et al.</i> (1995)
UCam	420–546	p, r	600	4.0	CCD	–55	1132	yes	no	no	1.0	9	≪1	no	–	Aliwell and Jones (1997)

^a Plus the 5 standard Brewer wavelengths for UV-ozone.

^b Brewer in original 5-wavelength mode assumes fixed wavelengths, so interpolation error from small sampling ratio does not arise.

^d Most temperature-stabilised instruments were overheating at times.

p = plane; c = concave; r = ruled; h = holographic; S = signal; R = reference.

Ret = EG&G Reticon diode array; NMOS = Hamamatsu NMOS (CCD semiconductor technology) 1-D array; CCD = 2-D array; PMT = photomultiplier tube; G-T = Glan-Thomson.

Table II. Dates in June 1996 when no slant columns of O₃ and NO₂ were deduced during the NDSC UV-visible intercomparison campaign, and reasons for not doing so

Group and instrument	Date in June 1996										
	11	12	13	14	15	16	17	18	19	20	21
	p	a p	a p	a p	a p	a p	a p	a p	a p	a p	a
Aber	-	- b	b -	- n	- n	- n	r r	- -	- -	- -	-
AES7*	c	c c	- -	- n	- n	- n	- -	- -	- -	d -	-
AES22*	c	c c	- k	- n	- n	- n	k -	- -	- -	d k	k
Brem	-	- -	- -	- n	- n	- n	- -	- -	- -	- -	j
CNR	-	- -	- -	- n	- n	- n	e -	q q	- -	- -	-
CNRS1	-	- b	b -	- n	- n	- n	- -	- -	- -	- -	-
CNRS2	-	- -	- -	- n	- n	- n	- -	- -	- -	- -	-
CNRS3	-	- -	- -	d n	d n	- n	- -	- -	- -	- -	-
Heidv	-	- -	- -	- n	- n	- n	f -	- -	- -	- -	-
HeidU	-	- -	- -	- n	- n	- n	f -	- -	- -	- -	-
IASB	-	- -	- -	- n	- n	- n	- -	- -	- -	- -	-
INTA**	g	g -	- -	- n	- n	- n	- -	- -	- -	- -	-
NILU1	-	- -	- -	e n	e n	- n	- -	- -	- -	- -	-
NILU2	-	h h	h h	- n	h n	h n	h h	h -	- -	- -	-
NIWA	-	- -	- -	- n	- n	- n	- -	- -	- -	- -	-
UCam	c	c c	c c	c n	m n	- n	i -	- i	i s	s s	s

b = Swapping parts to investigate fault in NILU2, refocussing.

c = Instrument arrived after start, being installed.

d = Computer crash probably due to mains-power interruption.

e = Automatic program operation interrupted in error.

f = Sun-shade to remove direct sun signal fell over optics during storm.

g = Condensation on detector window due to unusual heat and humidity.

h = Fault from computer earth via site UPS, plus overheating symptoms.

i = Faulty connector on detector data-link caused intermittent program stalls.

j = Baffle left over aperture after laser measurements at night.

k = Fast-moving cloud, which gives noisy spectra with slow-scan spectrometer.

m = Wrong wavelength range selected in error.

n = Afternoon removed because of excessive cloud cover.

q = No specific reason for missing single reference data.

r = No specific reason for missing daily reference data.

s = Daily reference spectrum not measured.

* NO₂ single reference data only.

** NO₂ data only.

3. Instrument Characteristics

Technical details of the instruments are summarised in Table I. Note that the wavelength ranges given in Table I are those over which the instrument samples, not those over which spectra are analysed for O₃ and NO₂ given in Table V. In the AES and NIWA instruments, the spectrum from a grating is measured at single wavelengths by a photomultiplier tube (PMT), the spectrum being obtained by scanning the grating, or in the case of AES7, being sampled at discrete wavelengths by means of a mask. All other instruments contain a grating spectrometer which images the spectrum onto an array detector. Some detectors are cooled in order to reduce dark current and so increase the signal-to-noise ratio at low light levels.

The spectral resolution of instruments varies between 0.6 and 1.8 nm full-width at half maximum (FWHM). Narrower resolution increases the sensitivity to NO₂ because of its fine structure, but reduces the sampling ratio of pixels within the resolution. Because the measured spectrum must be divided by the reference spectrum before analysis, it must be interpolated to the pixel grid of the reference spectrum. A small sampling ratio increases the error when interpolating, and so the choice of spectral resolution is a compromise between sensitivity to NO₂, interpolation error, and spectral range (Roscoe *et al.*, 1996). In some instruments, temperature stabilisation minimises drifts in wavelength calibration. This minimises the degree of interpolation and so the interpolation error; it also minimises the influence of gain variations between adjacent pixels of an array detector because the gain cancels if there is no interpolation.

As required in the NDSC UV-visible protocol, spectral response functions were measured with Hg lamps and diffusers (see Figure 1 for an example). Because cross-sections must be smoothed by these spectral response functions before spectra can be analysed, it is important that they be measured accurately, as well as confirming that they have sufficient spectral resolution for sensitivity to NO₂. The response function in the SAOZ spectrometer in Figure 1 is dominated by the blur circle from the simple concave mirror-grating, and is well approximated by a Gaussian.

In a new development, some instruments measured response to Laser light, either HeNe or doubled or tripled YAG, provided by the Lidar group at OHP. For the first time for most instruments, this gave accurate upper limits to stray-light rejection, as illustrated in Figure 2. As expected, the figure shows that stray-light rejection exceeds 10⁴ for this instrument. It also shows that, to make accurate measurements if stray-light rejection were to exceed 10⁵, a longer averaging time would be needed – measurements well away from the laser line in Figure 2 merely display the quantisation levels of the instrument's analogue-to-digital converter.

Light scattered from a clear zenith sky is strongly polarised, so that instruments must select one plane of polarisation and track the sun, or be insensitive to polarisation. Instruments of the SAOZ design, which uses a concave grating and comparatively low resolution, rely on the grating's lack of polarisation response. Other unpolarised instruments used optical fibres to scramble the input polarisa-

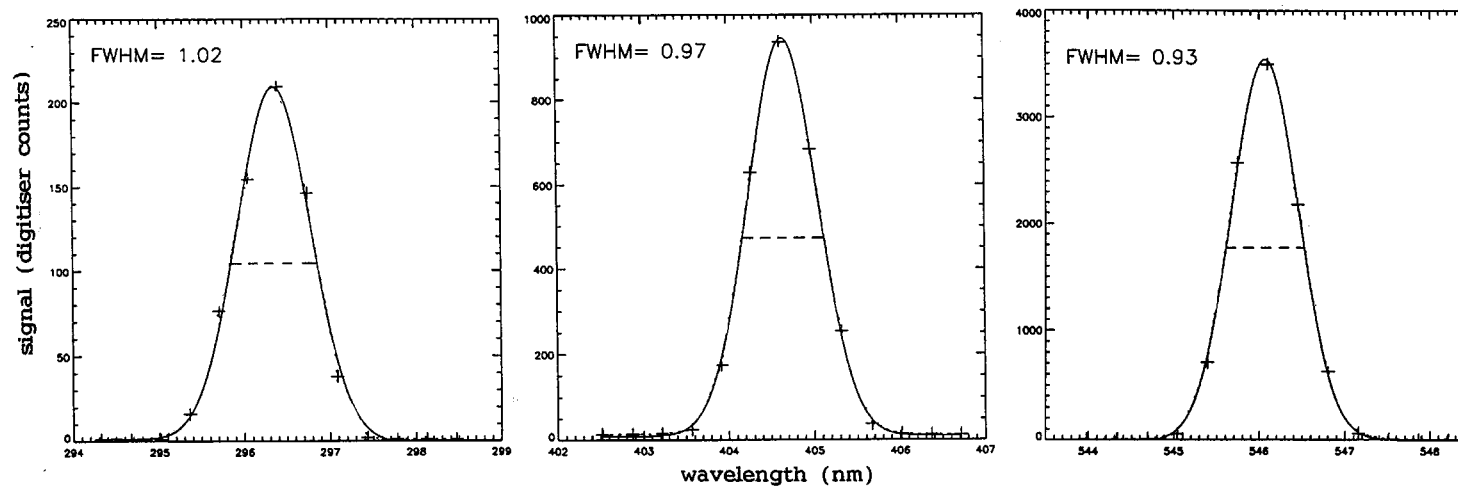


Figure 1. Spectrum of a low-pressure Hg lamp, recorded by the NILU2 spectrometer at OHP in June 1996, in the vicinity of each of the singlet Hg lines. Plus symbols show signals calculated from the Gaussian fitted to each line. The dashed lines show the full width at half maximum (FWHM) of the Gaussian fitted to each line, whose value in nm is stated above each line. Although 296 nm is outside the wavelength ranges used for O₃ or NO₂ analyses, the line at 296 nm is shown here to illustrate the degree of constancy of the spectral response function over the full wavelength range of the spectrometer.

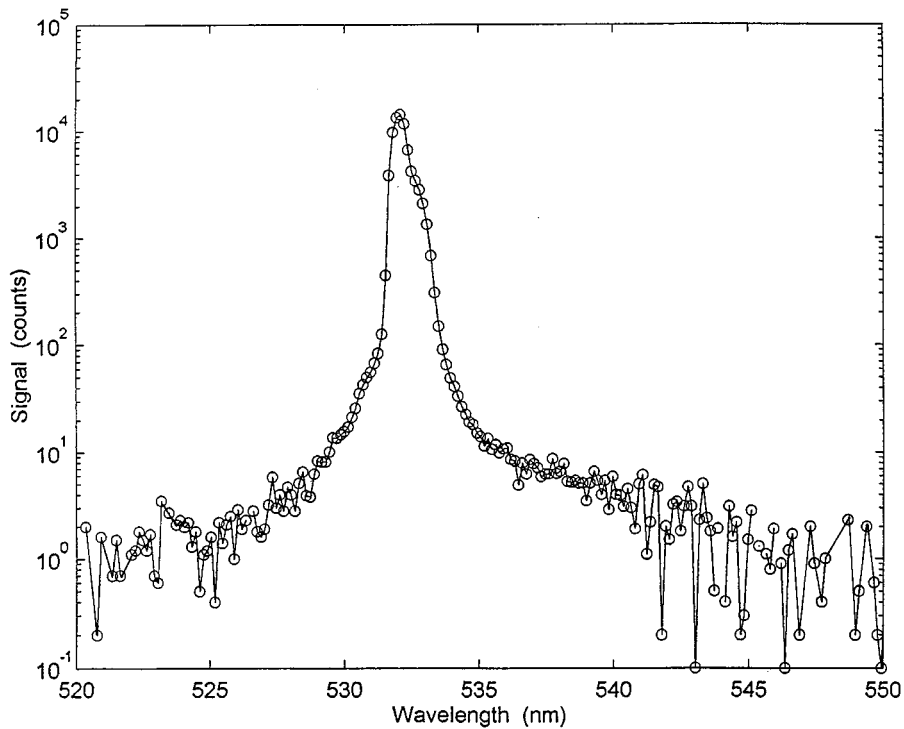


Figure 2. Spectrum of a doubled Nd-YAG Laser recorded by IASB spectrometer during the intercomparison campaign in June 1996.

tion. Individual glass or quartz fibres have a small diameter compared to their length, and so their depolarisation is excellent; sufficient throughput is achieved by using a bundle of fibres, although some signal is lost in the small gaps between the circular fibres in a bundle. Earlier experience of noise when moving glass fibres has been eliminated by modern packaging and termination, and in any case depolarised zenith-sky instruments need not move. Liquid light-guides are often used in UV instruments because they may have better transmission than glass at UV wavelengths and are cheaper than quartz; because they can have an arbitrarily large diameter, and so can be a single fibre with no gaps between adjacent fibres in which signal is lost; and because they are inherently noise-free. Unfortunately, we might expect a lesser depolarisation because of the larger diameter of liquid light-guides. Nevertheless, the depolarisation of a light-guide of diameter 8 mm and length 1 m was measured by CNR group to be 85 to 90% between 405 and 465 nm.

The lack of significant polarisation response in the unpolarised instruments was confirmed by measurements at the site, as also required in the NDSC protocol. A linear polariser was used during hazy sky near noon, and results are summarised in Table III. As expected, instruments using a fibre had negligibly small polarisation

Table III. Measurements of polarisation during the NDSC UV-visible intercomparison campaign in June 1996: mean ratio of maximum to minimum intensities with a film polariser in two directions at right angles, together with the maximum changes in this ratio with large (30 nm) and small (5 nm) changes in wavelength. Note the directions of the polarisers are not necessarily parallel and perpendicular to the slit or the grating grooves, because of internal mirrors

Group and instrument	Tungsten lamp			White sky		
	Mean	Change with large small changes in wavelength		Mean	Change with large small changes in wavelength	
Aber				1.05	0.06	0.02
AES7				Tracks solar direction		
AES22				Tracks solar direction		
Brem				1.05	0.004	0.001
CNR	1.6	0.6	0.4	1.0	0.6	0.4
				(Polarised, tracks solar direction)		
CNRS2				1.02	0.12	0.04
CNRS3				1.04	0.07	0.05
Heidv	1.02	0.015	0.005	1.05	0.01	0.01
HeidU	1.03	0.02	0.005	1.05	0.01	0.005
IASB				1.22	0.01	0.002
				1.25	0.01	0.002
INTA	1.15	0.2	0.07	1.12	0.2	0.07
NILU1				1.01	0.005	0.002
NILU2				1.02	0.06	0.04
NIWA				Polarised, tracks solar direction		

response. SAOZ also had a small response, with the lower-resolution SAOZ (Aber) having a smaller response than the higher-resolution versions.

There were several instruments and analyses of the SAOZ design: Aber, CNRS1, 2 and 3, and NILU2. Most SAOZ instruments are run and analysed by an HP desk-top computer. Aber is the only remaining SAOZ-512 (512 pixels, hence small sampling ratio) in the SAOZ network except the SAOZ at Faraday in Antarctica; CNRS1 is the analysis of Aber results with a PC version of the analysis software, similar to that used for Faraday results. CNRS3 is a new version of SAOZ-1024 which is run and analysed by a PC.

One instrument (HeidU) is measuring exclusively at UV wavelengths, where there is more information on height profiles of O₃ by the well-known Umkehr method, and of NO₂ (e.g., Preston *et al.*, 1997). One disadvantage for this intercomparison is that the AMFs are much smaller at these shorter wavelengths because of the higher altitudes of the mean scattering height at any one solar zenith angle, so

Table IV. The various types of slant column data requested from each instrument during the NDSC UV-visible intercomparison campaign in June 1996. The types are characterised by the letter used in data filenames. The daily reference spectrum was at 10:00 UT, except for 09:00 UT on 18 June. The single reference spectrum for the campaign was 09:00 UT on 18 June 96, except that CNR was forced to use 11:32 UT on 15 June, and NILU2 was forced to use 09:30 UT on 18 June, for operational reasons. The elevation of the sun was $>30^\circ$ after 09:00 UT

Filename letter	Gas	Dates in June 1996	Reference spectrum	Cross-sections
D	O ₃ and NO ₂	11 pm to 21 am	Daily	Preferred by instrument
S	O ₃ and NO ₂	11 pm to 21 am	Single	Preferred by instrument
R	O ₃ and NO ₂	19 am ^a	Single	Graham and Johnston
L	NO ₂	19 am ^a	Single	Graham and Johnston for O ₃ Coquart <i>et al.</i> (1995) at 220 K for NO ₂
W ^b	NO ₂	19 am ^a	Single	Graham and Johnston O ₃ and NO ₂

^a Only 18 am could be used by UCAM, making intercomparison difficult.

^b Wavelength range of the analysis restricted to 431 to 454 nm – other analyses used the range preferred by each group and listed in Table V.

that the instrument sees a smaller slant column despite observing the same vertical column.

4. Slant Column Results

Each instrument used its own software for analysing spectra, details of which are given in the references in Table I. Most instruments use the Fraunhofer lines in the reference spectrum to calibrate wavelengths, then use the spectral fitting procedure to determine the wavelengths of the measurement spectrum. Bremen and CNR, however, use a spectral lamp to determine the wavelengths of the reference spectrum.

In order to better assess the reasons for differences between instruments, several analysis protocols were used by all instruments, as listed in Table IV. Spectra were analysed using both daily reference spectra and a single campaign reference spectrum – a single reference is more useful when examining trends in a long series of data, whereas a daily reference might have smaller changes in wavelength calibration and so smaller interpolation errors. Some instruments experienced difficulties in wavelength stability relative to a single campaign reference, because of hot weather in the afternoons, when instruments exceeded their stabilisation temperatures. In the case of Bremen, whose spectrometer is normally very stable, there had been no experience in coping with large drifts in wavelength calibration, so that preliminary analyses with a single reference were of poorer quality than

Table V. Cross-sections used for measuring O₃ and NO₂ during the NDSC UV-visible intercomparison campaign in June 1996

Group and instrument	NO ₂ cr-sec	NO ₂ int. (nm)	O ₃ cr-sec	O ₃ int. (nm)	O ₄ cr-sec	O ₄ int. (nm)	H ₂ O cr-sec	H ₂ O int. (nm)
Aber CNRS1	G & J	412–426 & 434–498	G & J	450–580 & 556–584	Gb	465–484 & 560–605	SAOZ ground	496–520
AES7	G & J	426–456	B & P	310–320	–	–	–	–
AES22	G & J	426–456	G & J	as NO ₂	–	–	–	–
Brem	GOME	450–500	GOME	450–500	Gb	as NO ₂	HI	as NO ₂
CNR	CNR	407–464	G & J	437–464	Gb	as NO ₂ & O ₃	HI	as NO ₂ & O ₃
CNRS2,3	Meri	405–498	G & J	450–516	Gb	440–520	SAOZ	435–560
NILU2			Brio	516–580		& 550–626	ball	560–626
Heidv	Coqu	400–420 & 428–466	A & M	450–555	Gb	as O ₃	HI	as O ₃
HeidU	GOME/ Meri	345–358	Brio	328–340	–	–	–	–
IASB	VD	415–455	G & J	470–540	Gb	as NO ₂ & O ₃	HI	as NO ₂ & O ₃
INTA	G & J	430–470	G & J	450–540	Gb	450–540	HI	450–540
NILU1	G & J	415–455	G & J	428–480	Gb	as NO ₂ & O ₃	HI	as NO ₂ & O ₃
NIWA	Hard	437–470	GOME	as NO ₂	Gb	as NO ₂	NOAA	as NO ₂
UCam	Hard	420–450	G & J	450–525	Gb	as NO ₂ & O ₃	HI	as NO ₂ & O ₃

G & J = Graham and Johnston, unpublished, room T.

B & P = Bass and Pauer (1985).

A & M = Anderson and Mauersberger (1986).

H & J = Harwood and Jones (1994), low T.

Gb = Greenblatt (1994).

HI = HITRAN (Rothman *et al.*, 1992).

Coqu = Coquart *et al.* (1995), low T.

Meri = Merienne *et al.* (1995), room T.

Brio = Brion *et al.* (1993), low T.

VD = Van Daele *et al.* (1996), room T.

GOME = GOME flight model + White cell (Burrows *et al.*, 1998 and unpublished), scaled to H & J (NO₂) at 243 K, and to B & P (O₃) at low T.

Hard = Harder *et al.* (1997), low T.

CNR = measured by CNR spectrometer, scaled to Lauder values.

those with a daily reference. These standard analyses (types S and D in Table IV) used the cross-sections given in Table V.

Figure 3 is typical of the degree of agreement between NO₂ results during the morning. Some show variation whilst others change smoothly with SZA. However, during afternoons this smooth progression of slant columns was frequently disturbed by very thick clouds, which often became thunderstorms late in the afternoon. Multiple scattering in clouds enhances tropospheric path lengths so that slant columns of O₃, NO₂, H₂O and O₄ are increased (Erle *et al.*, 1995). In summer at OHP, smog is often associated with the meteorological conditions which create thunderstorms, which combines with the enhanced path lengths to give the very large increases in slant columns of NO₂ typified in Figure 4, and large

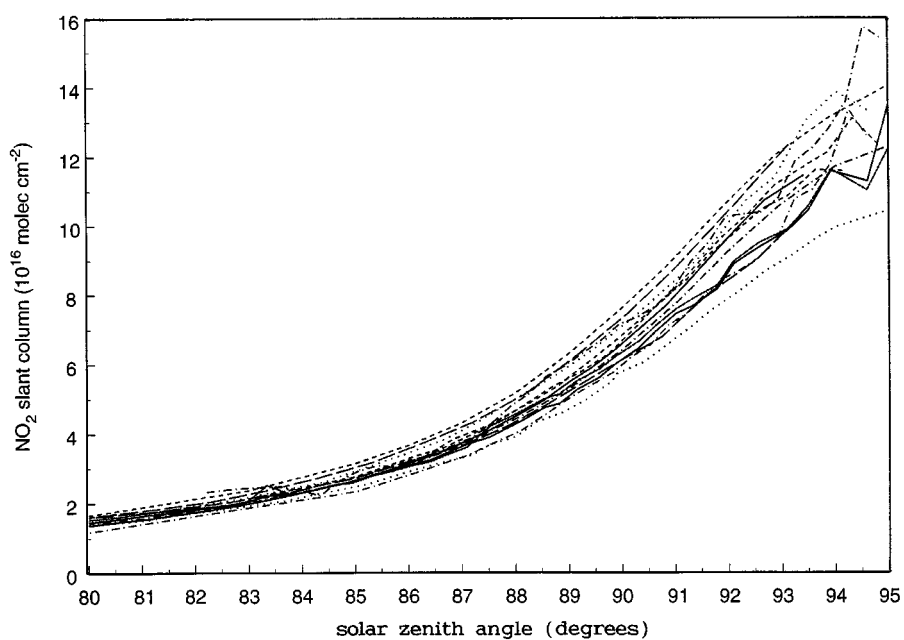


Figure 3. Slant columns of NO_2 measured by the various instruments in the intercomparison campaign on the morning of 12 June 1996.

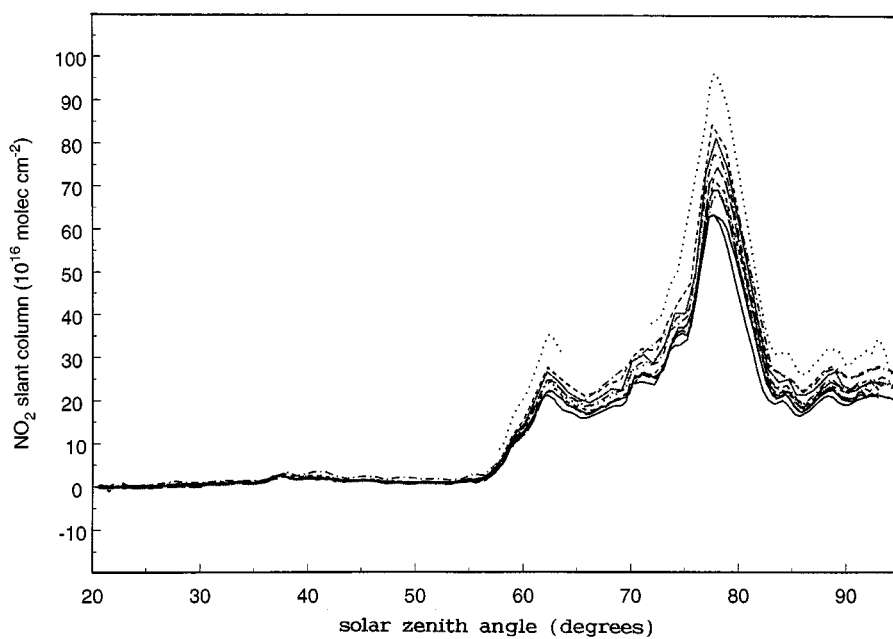


Figure 4. Slant columns of NO_2 measured by the various instruments on the afternoon of 15 June 1996, illustrating significant path enhancement in a cloud together with enhanced tropospheric NO_2 due to photochemical smog.

increases in those of O₃. Because of the differences between the diurnal cycles of NO₂ and O₃ in the polluted troposphere, increases of O₃ were usually seen only in the mid-afternoon near solar zenith angles (SZAs) of 40 to 50°, whereas the enhancements in NO₂ were more typically at SZAs of 60 to 85°, at the height of any thunderstorm activity, and where they might affect the routine derivation of vertical columns of NO₂. Differences in analysis procedures between instruments often create differences in apparent path-length enhancement, and non-uniformity of the clouds together with differences in field-of-view will result in differences in actual enhancement, so that several afternoon measurement sets were eliminated from the intercomparison, as listed in Table II.

Each instrument group supplied sample plots of fitted cross-sections and residuals, both for a twilight spectrum and a spectrum at high sun. Figure 5 shows a typical set of fits. From these plots, it became clear that integration time and smoothing must be specified in order to make a more meaningful comparison of the results. Instruments with cooled array detectors had a 5 to 10-fold reduction in residuals between an SZA of 90° and an SZA of 30°, but those with uncooled array detectors (CNRS, Aber) had only 2-fold reduction, so they are being limited by detector noise at high sun, presumably read-out noise. Although we only concerned ourselves with residual measurements up to SZA 90°, the size of residuals in NO₂ data at solar zenith angles greater than 90° is also particularly important for profiling of NO₂ (e.g., Preston *et al.*, 1997). Finally, some instruments did not supply fits to Ring cross-sections, an important omission because of the large optical depth of the Ring cross-sections.

Two methods for comparing slant columns between instruments were used:

(a) Regression analyses against a comparison instrument were performed over the whole range of SZAs available during each half-day (the range was different for each instrument and each half-day). This provided excellent displays of the nature of disagreements, allowing diagnoses of possible sources of error. Including small SZA (and so small slant column) in the NO₂ comparison should also be particularly useful in assessing potential performance when deployed in polar regions, where NO₂ amounts are small in winter. Note that a wide range of slant columns, and so of SZA, is essential in order to determine slope and intercept of correlation plots.

(b) Fractional differences from a comparison instrument were found over a fixed range of SZAs at twilight during each half-day, and the results averaged over the whole campaign. We chose the range 85° to 91° because this gave a smaller standard deviation than, say, 80° to 91°, and noise on the average was less than for a very narrow SZA range (say, 89.5° to 90°); and because fractional errors in slant columns are smallest in this range (Hofmann *et al.* 1995) – for this reason this is the range used by most groups for deducing vertical columns.

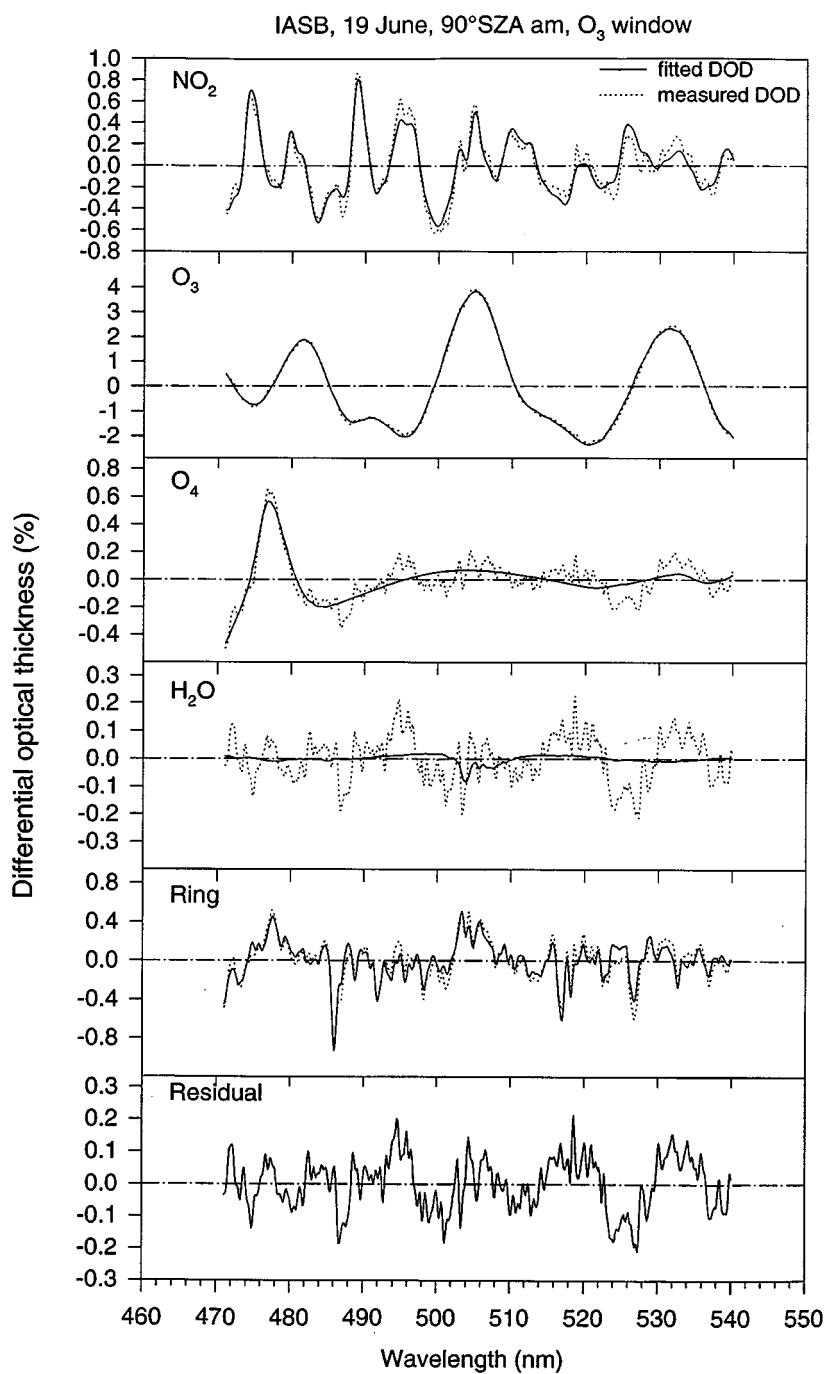


Figure 5. Fitted differential cross-sections, differential optical depths and residuals, measured by the IASB instrument during the morning twilight of 19 June 1996.

4.1. REGRESSION ANALYSIS

Here, we developed an important new way to compare results when no one instrument is known to be better than others. To investigate how closely a set of results from one instrument (the X set) match those from another (the Y set), we used a linear regression analysis to remove the offset and linear differences between them. This allowed us to plot residuals as well as to find the usual slope and intercept of the regression. Systematic errors due to correlation of the wanted cross-section with cross-sections of other absorbers, or with artifacts in the spectrum, would have a different dependence on SZA than that of the wanted absorber. Hence we can expect both non-zero intercept and a non-unity slope from regressions with systematic errors. If these errors are small, then a linear regression should be sufficient for their characterisation. These errors will vary with choice of wavelength interval, the method used to handle the Ring effect, and other spectral analysis factors.

Because each data set covers a different SZA range and has a different SZA spacing, both sets are first transformed onto a common SZA (Z) grid of spacing 0.2° and with range common to both sets, using a cubic interpolation. The interpolated results (Z_i, X_i, Y_i) are analysed using the regression method given in Hald (1952). The equation fitted is:

$$Y = \text{Intercept} + \text{Slope} \times X .$$

From this equation, one can derive the residuals R_i , where:

$$R_i = (\text{Intercept} + \text{Slope} \times X_i) - Y_i .$$

Residuals are plotted as a function of SZA , for visual study of the difference between the sets. Matrices of the regression parameters – residual error (standard deviation of R_i), slope and intercept – were generated for selected half days, for the regression of each instrument's results (as the dependent Y set) against the results of all other instruments (as the independent X set). For the 16 participating instruments these matrices contain 16×16 values, which gives 240 potentially useful values for each of the three regression parameters. An example of the regression matrices used in this selection is given in Table VI. This regression analysis is for the 19 June am NO₂ data set which was analysed using the participants' preferred cross-sections and wavelength intervals. The matrices include the conjugate values to enable comparison of results when the dependent and independent sets are exchanged. As expected, after allowing for the reciprocating of the slope and the reversing of the intercept sign, the conjugate values differ only slightly when errors are small. Although the slope matrix was not used to select the three reference instruments it is included to show the range of values found, from a maximum of 1.73 to a minimum of 0.63 (right half matrix). The residual errors range from nearly 1.9 to less than 0.03×10^{16} molec cm⁻², and the intercepts range from ± 1 to less than $\pm 0.01 \times 10^{16}$ molec cm⁻². The errors on the slopes and intercepts have been

Table VI. Results of regression analyses of NO₂ data from the morning of 19 June, analysed using the single campaign reference, with solar zenith angles greater than 70°. Instrument identifications are: Aber = A; AES7 = B; AES22 = C; Brem = D; CNR = E; CNRS1 = F, CNRS2 = G; CNRS3 = H; Heidv = I; HeidU = J; IASB = K; INTA = L; NILU1 = M; NILU2 = N; NIWA = O

(Y)	X=A	B	C	D	E	F	G	H	I	J	K	L	M	N	O
Residual error matrix (10 ¹⁶ molec cm ⁻²)															
A		0.773	0.358	0.067	0.078	0.192	0.120	0.135	0.125	0.375	0.049	0.072	0.047	0.170	0.115
B	0.847		0.890	0.533	0.492	0.993	0.498	0.623	0.815	0.653	0.580	0.547	0.535	0.661	1.720
C	0.426	0.887		0.214	0.175	0.463	0.211	0.353	0.474	0.655	0.414	0.226	0.206	0.292	0.437
D	0.078	0.518	0.214		0.036	0.257	0.160	0.046	0.078	0.337	0.041	0.043	0.059	0.239	0.028
E	0.078	0.398	0.146	0.032		0.221	0.046	0.032	0.073	0.115	0.042	0.039	0.058	0.039	0.038
F	0.195	0.884	0.394	0.226	0.235		0.205	0.277	0.192	0.358	0.204	0.232	0.205	0.177	0.242
G	0.143	0.527	0.212	0.165	0.058	0.236		0.180	0.145	0.293	0.136	0.191	0.131	0.257	0.166
H	0.145	0.563	0.324	0.042	0.033	0.296	0.159		0.186	0.442	0.125	0.045	0.065	0.234	0.141
I	0.139	0.799	0.447	0.077	0.084	0.211	0.138	0.196		0.363	0.080	0.085	0.055	0.228	0.167
J	0.296	0.449	0.412	0.249	0.107	0.269	0.205	0.339	0.265		0.280	0.263	0.228	0.396	0.282
K	0.062	0.615	0.438	0.045	0.054	0.252	0.144	0.147	0.090	0.429		0.068	0.042	0.232	0.043
L	0.082	0.519	0.222	0.042	0.043	0.259	0.182	0.049	0.084	0.347	0.061		0.073	0.237	0.037
M	0.048	0.456	0.179	0.052	0.059	0.203	0.112	0.063	0.049	0.271	0.034	0.065		0.220	0.049
N	0.250	0.794	0.376	0.293	0.051	0.270	0.327	0.319	0.295	0.778	0.266	0.295	0.316		0.274
O	0.126	1.612	0.399	0.026	0.041	0.265	0.151	0.142	0.164	0.371	0.037	0.036	0.052	0.209	
Slope matrix (dimensionless)															
A		0.887	0.833	0.859	1.000	0.987	0.837	0.927	0.899	1.254	0.795	0.875	0.979	0.679	0.910
B	1.064		0.965	1.014	1.206	1.073	0.930	1.089	0.996	1.431	0.931	1.037	1.156	0.801	0.975
C	1.180	0.956		0.994	1.195	1.162	0.992	1.083	1.050	1.556	0.937	1.013	1.146	0.769	1.086
D	1.164	0.957	1.000		1.151	1.134	0.970	1.103	1.016	1.340	0.918	1.023	1.137	0.810	1.065
E	0.998	0.789	0.829	0.868		0.929	0.799	0.958	0.870	1.067	0.789	0.900	0.972	0.764	0.925
F	1.009	0.850	0.843	0.875	1.055		0.866	0.931	0.911	1.322	0.806	0.891	1.005	0.653	0.913
G	1.192	1.043	1.002	1.027	1.251	1.147		1.134	1.046	1.424	0.946	1.047	1.171	0.782	1.094
H	1.077	0.890	0.912	0.907	1.043	1.063	0.879		0.948	1.290	0.851	0.928	1.031	0.730	0.991
I	1.111	0.957	0.932	0.983	1.147	1.094	0.953	1.050		1.364	0.896	1.006	1.119	0.770	1.019
J	0.783	0.675	0.617	0.735	0.933	0.744	0.695	0.758	0.724		0.648	0.752	0.837	0.490	0.755
K	1.258	1.046	1.050	1.089	1.267	1.234	1.055	1.173	1.115	1.520		1.114	1.239	0.867	1.165
L	1.142	0.934	0.980	0.977	1.111	1.112	0.951	1.078	0.993	1.308	0.897		1.111	0.798	1.040
M	1.021	0.839	0.867	0.879	1.027	0.988	0.852	0.969	0.893	1.179	0.807	0.899		0.693	0.936
N	1.462	1.155	1.278	1.221	1.308	1.518	1.262	1.353	1.284	1.893	1.143	1.240	1.425		1.307
O	1.097	0.856	0.904	0.939	1.080	1.089	0.911	1.007	0.979	1.304	0.858	0.961	1.068	0.758	
Intercept matrix (10 ¹⁶ molec cm ⁻²)															
A		-0.347	0.344	0.272	-0.548	-0.021	0.283	0.527	0.155	-0.722	0.207	0.518	0.227	0.788	0.218
B	0.703		0.662	0.515	-0.520	0.499	0.909	0.816	0.552	-0.392	0.471	0.776	0.461	1.100	0.688
C	-0.306	-0.164		0.135	-0.971	-0.342	-0.018	0.405	-0.111	-1.618	-0.050	0.417	0.002	0.887	-0.055
D	-0.314	-0.392	-0.103		-0.923	-0.312	0.040	0.244	-0.040	-0.711	-0.039	0.260	-0.037	0.427	-0.078
E	0.555	0.558	0.844	0.802		0.692	0.933	1.013	0.788	0.353	0.784	1.012	0.793	0.799	0.733
F	0.042	0.100	0.397	0.311	-0.661		0.232	0.625	0.168	-0.990	0.241	0.562	0.217	1.185	0.311
G	-0.328	-0.826	0.050	-0.030	-1.166	-0.232		0.217	-0.084	-0.987	-0.089	0.261	-0.081	0.847	-0.111
H	-0.559	-0.625	-0.310	-0.220	-1.057	-0.621	-0.179		-0.309	-1.007	-0.297	0.015	-0.254	0.204	-0.341
I	-0.165	-0.333	0.224	0.041	-0.899	-0.163	0.089	0.337		-0.745	0.017	0.297	0.004	0.693	0.022
J	0.630	0.378	1.192	0.562	-0.319	0.808	0.719	0.827	0.578		0.591	0.755	0.532	1.753	0.558
K	-0.259	-0.380	0.155	0.044	-0.992	-0.267	0.103	0.355	-0.017	-0.846		0.327	0.002	0.641	-0.051
L	-0.589	-0.629	-0.375	-0.253	-1.124	-0.586	-0.234	-0.015	-0.292	-0.946	-0.292		-0.290	0.114	-0.330
M	-0.231	-0.296	0.025	0.034	-0.812	-0.184	0.075	0.248	-0.002	-0.596	-0.001	0.262		0.571	-0.035
N	-1.097	-0.708	-1.008	-0.445	-1.040	-1.733	-0.973	-0.186	-0.812	-2.779	-0.670	-0.063	-0.726		-0.584
O	-0.233	0.149	0.148	0.073	-0.791	-0.306	0.112	0.350	-0.014	-0.682	0.044	0.317	0.038	0.499	

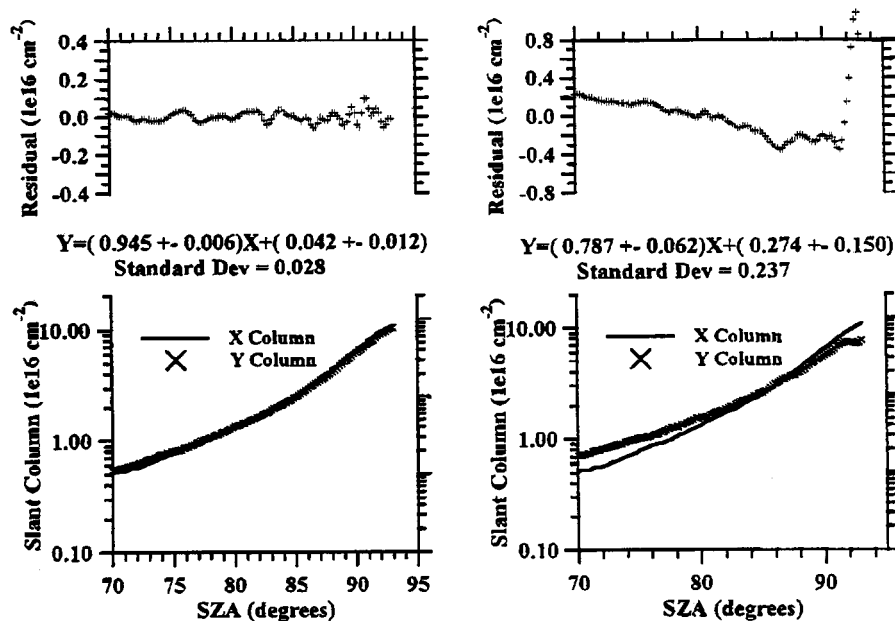


Figure 6. Typical plot of slant columns of NO₂ used by pairs of instruments in the regression analysis (lower figures), and the residual errors from the regression line (upper figures), for (a) instruments which agree well, and (b) instruments with significant disagreements. Note the log scale in the lower figures. The upper figures are excellent visual displays of the quality of the relative differences between the each pair of instruments.

calculated but not included, acceptable because they need only be smaller than the accuracy to which the instruments need to be compared. The comparison accuracy is discussed later.

To reduce the number of matrix values and plots we selected a small number of instruments to provide the independent X sets. Three instruments showed consistently smaller residual errors and intercept values for both O₃ and NO₂ – IASB, Bremen and NIWA – and so these were chosen as the comparison instruments. The slope values were not used in this selection because apart from one NO₂ twilight set, they are expected to vary because different cross-sections and wavelength intervals were used.

Regression plots have been generated for several of the measurement sets studied. Figure 6a shows an example of the regression between two instruments that are in good agreement. The top half of the plot shows the residuals R_i , which have a standard deviation (root mean square value) of 0.028, and the lower plot shows the measured data from each instrument. The example in Figure 6b shows much poorer agreement, with an inflexion at 86° SZA and large residuals beyond 92°.

Figure 7 and Table VII show the results of a second regression analysis on the 19 June am NO₂ data, this time analysed using a common wavelength interval and cross-sections and a single comparison instrument (NIWA). However, NIWA is

Table VII. NO₂ regression results for data from the morning of 19 June using the single campaign reference, with common analysis wavelength interval (431 to 454 nm), with solar zenith angles greater than 70°, and with Graham and Johnston cross-sections for NO₂ and O₃. Comparison is against NIWA

Instrument	Residual error (10 ¹⁹ molec cm ⁻²)	Slope (dimensionless)	Intercept (10 ¹⁹ molec cm ⁻²)
Aber	0.251	0.79	0.43
AES7	1.530	0.91	0.67
Brem	0.037	0.98	0.02
CNRS2	0.226	1.01	-0.46
Heidv	0.084	0.96	0.04
IASB	0.028	0.97	-0.05
INTA	0.072	0.95	-0.22
NILU1	0.045	0.75	0.03
NILU2	0.545	1.18	-1.85

polarised (see Section 3), and Fish and Jones (1995) showed that Raman scattering gives rise to an underestimation of NO₂ averaging 3.5% in unpolarised instruments (increasing to perhaps 4.7% at 90° SZA if multiple scattering is important), whilst underestimation of ozone is negligible. Hence the values of NO₂ from unpolarised instruments were scaled by 1.035 to compensate. This particular analysis and scaling removes most of the known causes of differences between instruments, so we expect a unity slope and a zero intercept.

In Table VII, several instruments agree to better than ±5% of unity in slope and show intercepts smaller than 0.06×10^{16} molec cm⁻². The residuals in Figure 7, combined with the residual error, slope and intercept values in Table VII, provide excellent diagnostic and assessment information for the NO₂ instrument intercomparison. The choice of NIWA as the comparison instrument was not determined by any perceived superiority over Bremen as the two instruments produce essentially identical results, but rather by the slightly larger maximum SZAs in the NIWA data.

Table VIII shows the regression results for O₃ averaged over all the mornings, with IASB as the comparison. Because results were averaged over the 10 campaign days, standard deviations are included. Although different wavelength intervals and cross-sections were used by each group, a number of groups agree to within ±5% of unity in slope. This contrasts to the NO₂ slopes for column O in Table VI, where the participants have a similar choice of data analysis parameters – only two instruments have slopes within ±5% of unity.

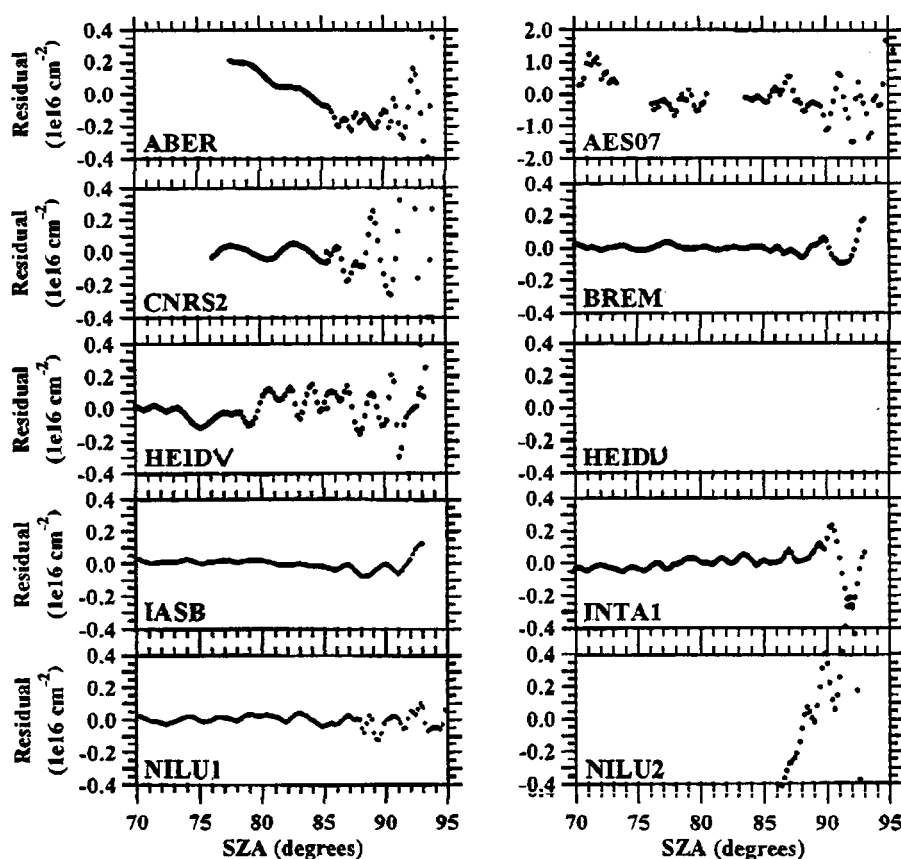


Figure 7. Residual errors from regression of NO₂ values derived on the morning of 19 June using Graham and Johnston room temperature cross-sections and a restricted wavelength range (431 to 454 nm). The comparison instrument was NIWA in each case.

4.2. FRACTIONAL DIFFERENCES

A sample plot of the evolution of fractional differences (see method (b) in Section 4 above) during the campaign is shown in Figure 8, where their consistency can easily be explored. To calculate these differences, because measurements by different instruments were not necessarily at the same solar zenith angles as those of the comparison instrument, they were linearly interpolated to the SZAs of the comparison instrument before subtraction. The bars in Figure 8 are the standard deviations of the fractional differences during each half-day. Because AMFs depend on wavelength, differences are expected if different wavelength regions are used – for example, HeidU, excluded from Figure 8, has much smaller values because it measures at UV wavelengths, where the AMFs are much less.

Averages and standard deviations of the fractional differences illustrated in Figure 8 were calculated from each valid half-day during the whole campaign. As comparison instruments, we chose the same three instruments which were iden-

Table VIII. O₃ regression results for all mornings using the single campaign reference, for solar zenith angles between 50° and 93°. Comparison is against IASB

Instrument	Residual error (10 ¹⁹ molec cm ⁻²)		Slope (dimensionless)		Intercept (10 ¹⁹ molec cm ⁻²)	
	Mean	Std. dev.	Mean	Std. dev.	Mean	Std. dev.
Aber	0.171	0.260	0.97	0.03	0.03	0.40
Brem	0.083	0.015	0.97	0.01	0.13	0.08
CNR	0.424	0.251	1.77	2.81	10.05	2.78
CNRS1	0.153	0.111	0.95	0.02	-0.06	0.51
CNRS2	0.137	0.065	0.96	0.03	0.37	0.14
CNRS3	0.118	0.021	0.99	0.02	0.04	0.21
Heidv	0.107	0.016	1.03	0.01	0.20	0.08
HeidU	0.533	0.104	0.52	0.04	0.64	0.09
NILU1	0.115	0.019	0.97	0.01	-0.05	0.11
NILU2	0.237	0.155	1.04	0.05	-0.42	0.36
NIWA	0.090	0.026	1.01	0.01	-0.08	0.10
UCam	0.107	0.022	1.08	0.01	0.36	0.27

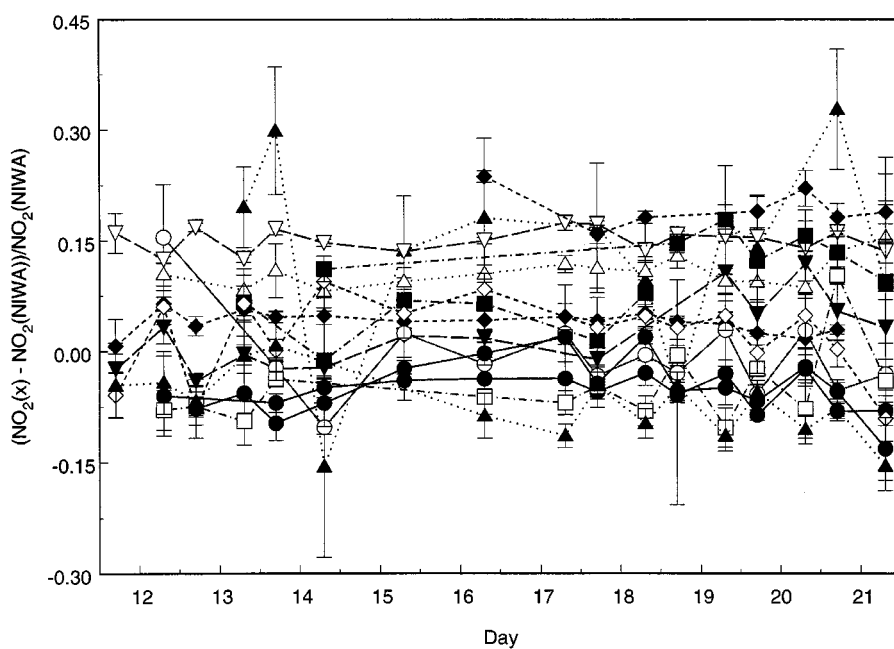


Figure 8. Fractional differences in NO₂ measured by each instrument from NO₂ measured by the NIWA instrument, averaged from 85° to 91° solar zenith angle, during the whole campaign at OHP in June 1996. Some afternoons when thick clouds gave enhanced NO₂, as in Figure 4, were excluded.

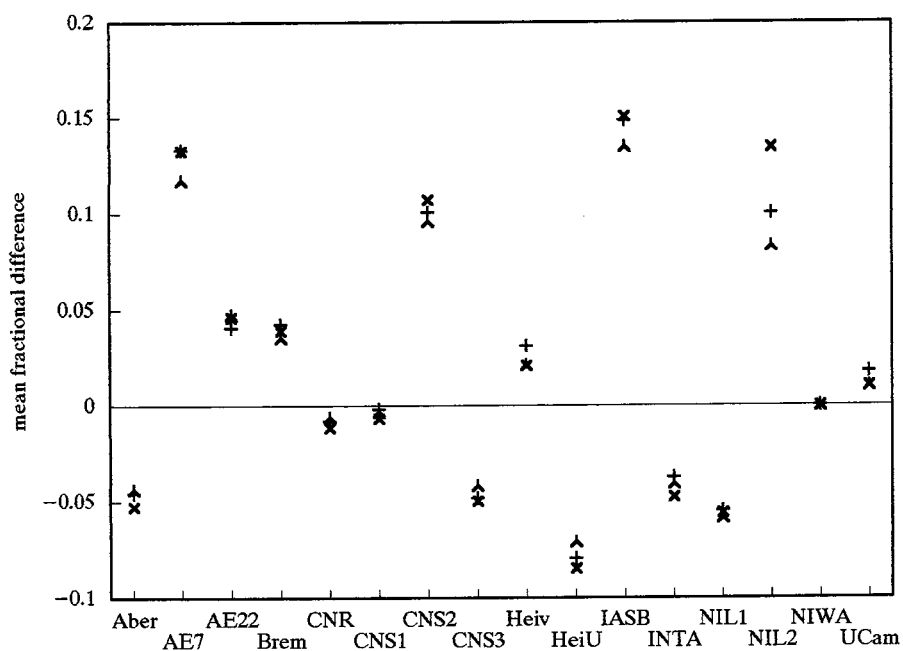


Figure 9. Mean fractional differences from each of the comparison instruments (Brem, IASB, NIWA) for the whole intercomparison campaign, for NO₂ analysed with a single campaign reference and averaged over the SZA range 85 to 91°. In order to investigate how the differences compare with different comparison instruments, they must be centred on one of the comparison instruments, chosen as NIWA here. The three symbols refer to the three different comparison instruments. Note that each comparison instrument gives similar results.

tified as the most useful comparison instruments during regression analyses. Figure 9 illustrates the consistency of these averages for each of the three comparison instruments – it matters little which of the three is used.

Averages and standard deviations were found separately for daily and single references, for both O₃ and NO₂. Figure 10 shows them for NO₂ with a daily reference, and illustrates that the results are very similar to those with a single reference in Figure 9. The standard deviations show that the scatter for NO₂ in Figure 10 is significant. For O₃, Figure 11 shows that the scatter is dominated by a single instrument and the scatter of the other instruments is barely significant.

Figures 10 and 11 illustrate the differences between instruments that would apply if one were to take values from instruments deployed at their own field sites, using their preferred cross-sections. However, we know that the cross-section of NO₂ varies significantly with temperature and that there are still important differences between recent low-temperature cross-sections (e.g., Harder *et al.*, 1997). Accordingly, we determined the correction factors between analyses using each preferred set of cross-sections and using cross-sections of Harder *et al.* (1997) at 227 K, by finding the slope of the line of regression between them after smoothing both the preferred cross-sections and those of Harder *et al.* (1997) by each

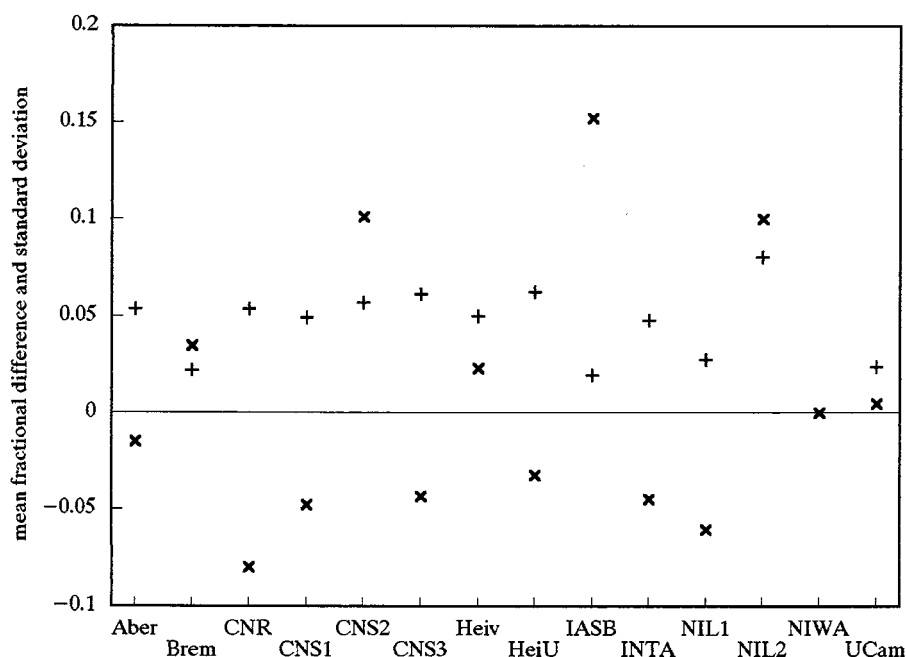


Figure 10. Mean fractional differences (\times) and standard deviations ($+$) from the comparison instrument NIWA for the whole intercomparison campaign, for NO_2 analysed with a daily campaign reference. The comparison is over the SZA range 85 to 91°. Note that HeiU should give somewhat smaller slant columns because of the shorter wavelengths used, which results in smaller AMFs.

instrument's slit function. Figure 12 shows the fractional differences for NO_2 after applying these correction factors, which are listed in Table IX. Comparing Figure 12 to Figure 10 shows a different pattern but a similar degree of scatter – the differences between instruments for NO_2 seem not to be dominated by their use of different NO_2 cross-sections. Some further reasons for the disagreements of Figure 12 are explored in Section 6. In the figure, we would expect HeiU to be smaller by the fractional difference in AMFs at 361 and 440 nm, averaged over 85 to 91° SZA, equal to 7.2%. A corrected value for HeiU in Figure 12 would then be +3.7%, making disagreement with the mean of the figure worse, for which we have no explanation.

We explored the significances of the fractional differences between instruments by examining how the standard deviations of each plot (the scatter), and the mean of the standard deviations of all instruments on each plot (the mean standard deviation), changed as instruments with large fractional differences were removed in turn. As outlying instruments were removed the values of the scatter were reduced, but eventually the reductions were small and the final value served as a figure of merit for the degree of agreement of the remaining instruments. If the mean

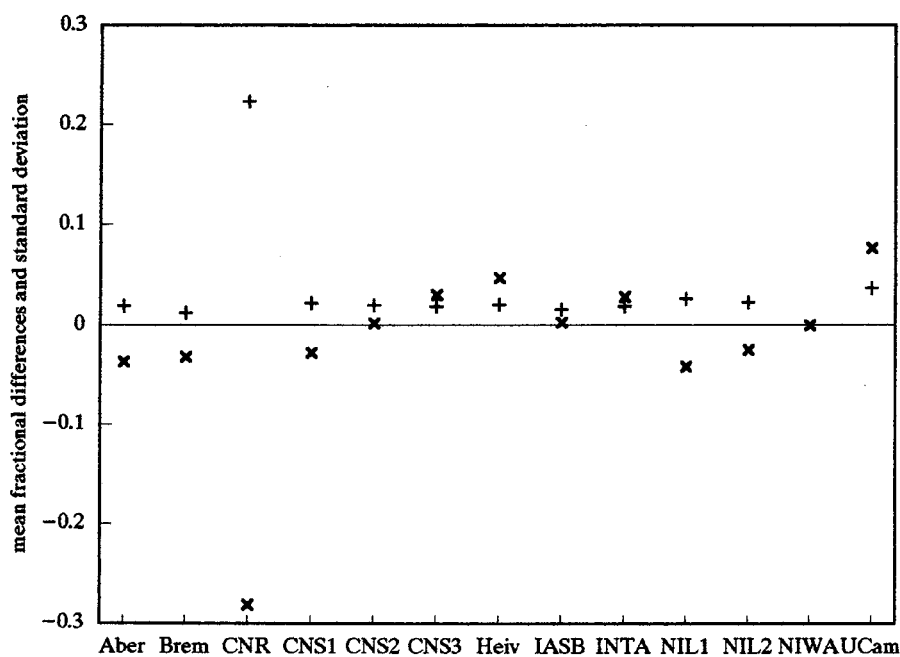


Figure 11. As Figure 10, but for O₃. HeidU is missing because, at its UV wavelengths, the AMFs and so slant columns are very much smaller than at the visible wavelengths of ozone observed by the other instruments.

standard deviations were not simultaneously reduced, this demonstrated that the differences were real differences between instruments.

For example, in Table X, successive eliminations reduce the rms scatter and average standard deviation simultaneously, so that differences in O₃ between instruments were probably not significant, although the reductions show that the quality of data from the first and second instruments eliminated was poor. By contrast, in Table XI, elimination did not reduce the average standard deviation, so that all the differences in NO₂ between instruments were real.

Interestingly, Table XI also shows that there was no reduction in scatter after correcting NO₂ measurements to the Harder *et al.* cross-sections (if anything the scatter increased slightly), so that differences between instruments do not seem to be an artifact of differences in the cross-sections used.

From Tables X and XI, we conclude that O₃ mean fractional differences for most instruments fall within $\pm 5.5\%$ (2 sigma), with standard deviations of the mean differences averaging 2%; and NO₂ mean differences for most instruments fall within $\pm 11.5\%$ (2 sigma), with standard deviations of the mean differences averaging 4.5%.

Table IX. Slope of the regression line between the NO₂ cross-sections used by each instrument and the low-temperature cross-sections of Harder *et al.* (1997), over the range 415 to 455 nm, after smoothing both cross-sections by the resolution function of each instrument. These coefficients can be used to scale the NO₂ measurements made by each instrument to approximate to the measurement that each would have made had each used the Harder *et al.* (1997) cross-sections

Instrument	Slope
Aber	0.853
AES7	0.837
AES22	0.837
Brem	0.904
CNR	1.000 ^a
CNRS	0.832
Heidv	0.969
HeidU	1.000 ^b
IASB	0.835
INTA	0.847
NILU1	0.835
NILU2	0.832
NIWA	1.000
UCam	1.000

^a Assumed values as original cross-sections unavailable but scaled to low temperatures.

^b Assumed values as instrument uses a different wavelength range.

5. Measurements with NO₂ Cells

Because of widespread confusion over NO₂ cross-sections and their temperature dependences in the past (e.g., Roscoe and Hind, 1993), and because of the possibility of incorrect diagnosis of stray-light rejection within an instrument, an important NDSC requirement is confirmation of accuracy by measurements of an NO₂ cell. A quartz cell of length 10 mm containing 8×10^{16} molec cm⁻² (about 3 mbar) of NO₂ and filled with O₂ to about one atmosphere was provided by the NOAA Aeronomy Lab, as described by Hofmann *et al.* (1995). A thermistor from the UCam group was attached to the cell. Some instruments made two sets of cell measurements on widely separated days, and the NIWA instrument made repeated measurements to act as a control. Instruments with internal access made trouble-free measurements, but it was difficult to organise shading with wide field-of-view instruments (e.g.,

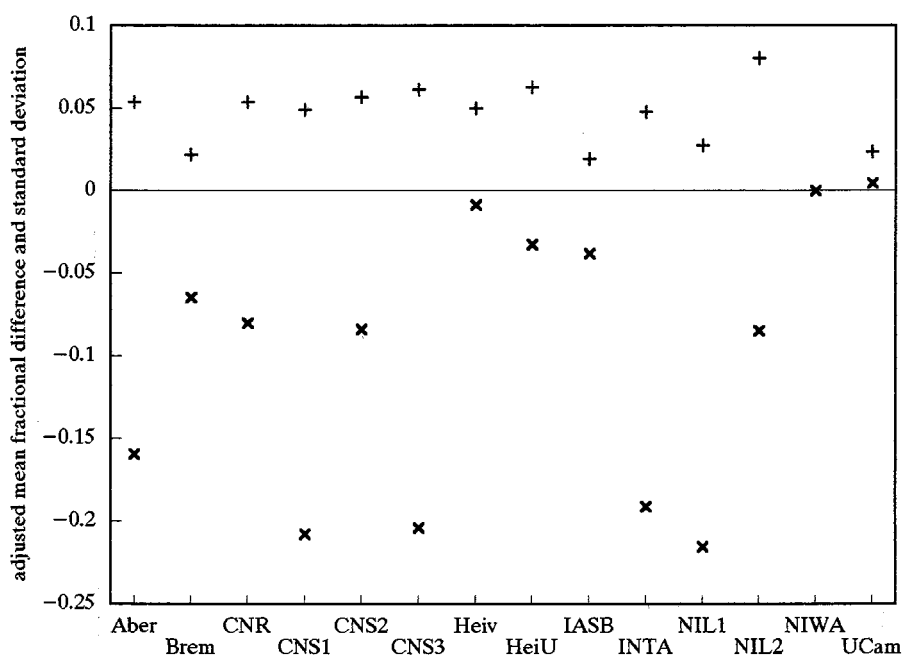


Figure 12. Mean relative differences from the comparison instrument NIWA for the whole campaign, for NO₂ analysed with a daily reference, after compensating for the different cross-sections used by each instrument using the scaling factors from Table IX.

Table X. Root-mean-square (rms) scatter and average standard deviation of fractional differences for O₃ for the whole campaign, as successive instruments are removed. Rms scatter is the standard deviation of each instrument's mean fractional difference. Average standard deviation is the average of the standard deviations from each instrument, each determined from the scatter of that instrument's fractional difference during all the valid half-days of the campaign. AES7, AES22, and INTA have no data for O₃. NIWA is excluded because it is the comparison instrument. HeidU is excluded because it uses very different wavelengths, so that AMFs are very different and one would not expect agreement in slant columns

	Reference spectrum	All insts.	First removal	Second removal	Third removal
Number of instruments	Both	12	11	10	9
Instruments excluded	Both	–	CNR	UCam	Heidv
Rms scatter	Single	0.275	0.042	0.031	0.025
Average std. dev.	Single	0.049	0.020	0.020	0.021
Rms scatter	Daily	0.086	0.037	0.030	0.026
Average std. dev.	Daily	0.038	0.021	0.019	0.019

Table XI. Rms scatter and average standard deviation (defined in Table X) of fractional differences for NO₂ for the whole campaign, as successive instruments are removed. AES7 and AES22 have no data for the NO₂ daily reference spectrum. NIWA is excluded because it is the comparison instrument. HeidU is excluded because it uses very different wavelengths, so that AMFs are very different and one would not expect agreement in slant columns. Harder is Harder *et al.* (1997). Note that IASB is using room-temperature cross-sections in order to conform to the standard SAOZ product, so that its large difference and so first removal is to be expected

	Cross-section	Ref. spect.	All insts.	First removal	Second removal	Third removal
Number of instruments	Both	Single	14	13	12	11
Instruments excluded	Original	Single	–	IASB	NILU2	AES7
Rms scatter	Original	Single	0.072	0.066	0.060	0.049
Average std. dev.	Original	Single	0.038	0.040	0.041	0.033
Instruments excluded	Corrected to Harder	Single	–	NILU1	CNRS3	Aber
Rms scatter	Corrected to Harder	Single	0.078	0.074	0.069	0.063
Average std. dev.	Corrected to Harder	Single	0.045	0.045	0.045	0.047
Number of instruments	Both	Daily	12	11	10	9
Instruments excluded	Original	Daily	–	IASB	CNRS2	NILU2
Rms scatter	Original	Daily	0.071	0.059	0.052	0.037
Average std. dev.	Original	Daily	0.041	0.043	0.042	0.043
Instruments excluded	Corrected to Harder	Daily	–	NILU1	CNRS1	CNRS3
Rms scatter	Corrected to Harder	Daily	0.077	0.074	0.069	0.061
Average std. dev.	Corrected to Harder	Daily	0.046	0.048	0.048	0.046

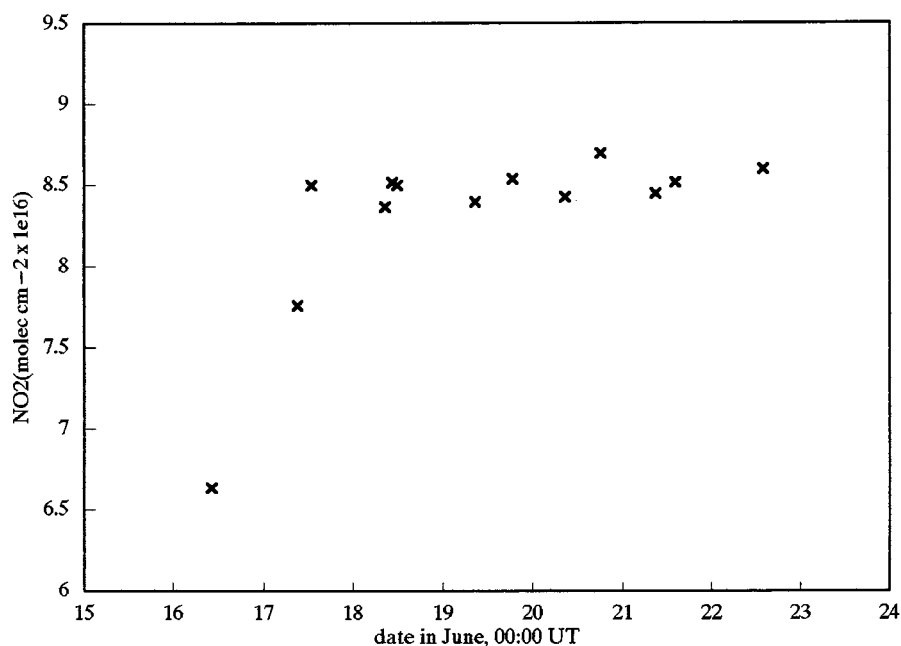


Figure 13. Measurements by the NIWA spectrometer of the amount of NO₂ in the cell during the course of the intercomparison campaign in June 1996.

SAOZ) which necessarily operated with the cell in daylight. A blank cell was also provided, and spectra with the blank were used as the reference when analysing cell spectra.

The amount of NO₂ in the cell changed by over 20% during the first few days of the campaign, as shown by the NIWA measurements in Figure 13. The eventual amount is very similar to the amount measured in 1992 in New Zealand, whereas there had been a steady reduction in the intervening years. We surmise that this slow adsorption of NO₂ onto deep-seated sites in the cell had been reversed by the occasional exposure to sunlight which was inevitable in making measurements with instruments with limited internal access. We determined the ratio of each cell measurement to that of NIWA on the same day, but unfortunately the pattern of the results bears little resemblance to the atmospheric measurements in either Figure 10 or Figure 12.

However, the temperatures of the cell were significantly different in each measurement, again inevitable in those instruments without temperature control or with limited internal access, particularly when measurements were made in mid-morning when the sky was usually clear and stable. Because the cell was made of quartz, we did not expect the significant short-term and highly temperature-dependant adsorptions typical of stainless-steel or titanium cells with glued or O-ring sealed windows, which can give temperature coefficients of several percent/degree (e.g., Roscoe and Wells, 1989). Instead, we merely expected the tem-

Table XII. Temperature coefficients of NO₂ amount in the cell from conversion between NO₂ and N₂O₄, from the formula of Roscoe and Hind (1993). Temperatures are those at which Vosper (1970) calculated the equilibrium constant. The proportion of NO₂ in the NO₂-N₂O₄ mixture is given by α , and the temperature coefficient is deduced from adjacent values of α

Temperature (°C)	α	Temperature coefficient (% K ⁻¹)	Mean temperature (°C)
0	0.7821		
8.7	0.8751	1.29	4.4
25.0	0.9591	0.56	16.9
35.0	0.9792	0.21	30.0

perature coefficient of NO₂ to N₂O₄ conversion (e.g., Vosper, 1970). Taking the formula and values from Roscoe and Hind (1993), this would give the temperature coefficients listed in Table XII.

At first, a plot of cell amount versus temperature seemed to have a much larger coefficient than in Table XII for the range of temperatures of the cell measurements (19 °C to 33 °C), although the scatter was as large as that of Figure 11. This was investigated more rigorously with the cell in the NIWA instrument, after their return to New Zealand, by placing the cell in a temperature-controlled water cooling jacket. Some results are shown in Figure 14, which shows a coefficient of about 0.43% K⁻¹ at 12.5 °C, slightly less than the value of 0.56% K⁻¹ at 16.9 °C in Table XII. Hence the apparently large coefficient was an artifact of cell measurements by instruments which measured less NO₂ being made at lower temperatures.

Accordingly, we applied corrections to the measured cell amount using the temperature coefficient of 0.45% K⁻¹, appropriate from Table XII for the mean cell temp. of 26 °C, as a correction to the cell measurements, and computed the fractional differences from NIWA. The questions then arise: do these fractional differences of cell measurements agree with the fractional differences of atmospheric measurements in Figure 12? If not, are the disagreements significant? Figure 15 shows the difference between these cell and atmospheric measurements, and compares them to the standard deviations in Figure 12. From Figure 15, we conclude that for most instruments, atmosphere and cell differ by less than 2 standard deviations, and no differences exceed 3 standard deviations. Hence the cell confirms the general conclusions, from the fractional differences, but has a similar degree of error.

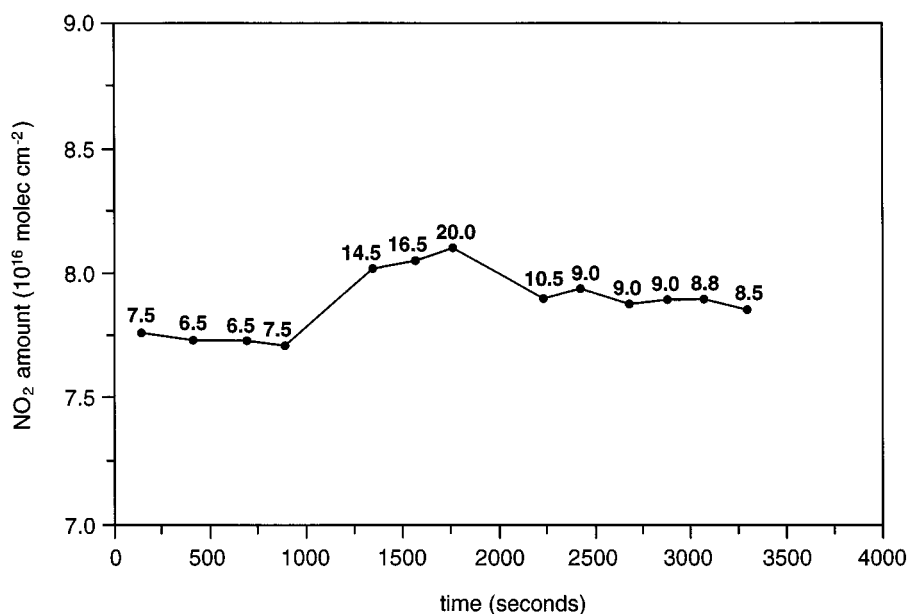


Figure 14. The amount of NO₂ in the cell, measured by NIWA, after installing a temperature controlled water jacket around the cell. Numbers on the figure are the cell temperatures (°C). Note the hysteresis in the cell amount.

6. Possible Sources of Error in NO₂ Slant Columns

Although there are many recent publications of NO₂ cross-sections, including their temperature dependence (e.g., Harder *et al.*, 1997), there are still significant discrepancies between different measurements in the literature. For this reason, many in the SCUVS consortium have chosen to analyse with room temperature cross-sections, preferably Graham and Johnston. This gives NO₂ slant columns which are about 15% too large (hence perhaps the difference between NIWA and IASB), but unfortunately the exact error depends on the spectral range and resolution. Hopefully, there will soon emerge a consensus on low-temperature cross-sections which can then be used by all instrument groups.

Because NO₂ has much finer spectral structure than O₃, errors in spectral response function give rise to much larger errors in NO₂ columns than in O₃ columns. For example, in an extreme case, the slope of the regression line for IASB against NIWA can be changed by 18% by reanalysing with a FWHM of 0.85 nm (as observed in IASB at 468 nm) instead of 1.04 nm (as observed in IASB at 435 nm). Future work by some of us will be aimed at determining the response function from the Fraunhofer lines in the spectra themselves, then fitting a function to interpolate between the wavelengths where it has been determined, and smoothing the cross-sections with this wavelength-dependent function.

The interpolation of the spectrum to a common pixel grid, which is essential before the measured spectrum can be divided by the reference spectrum (see Sec-

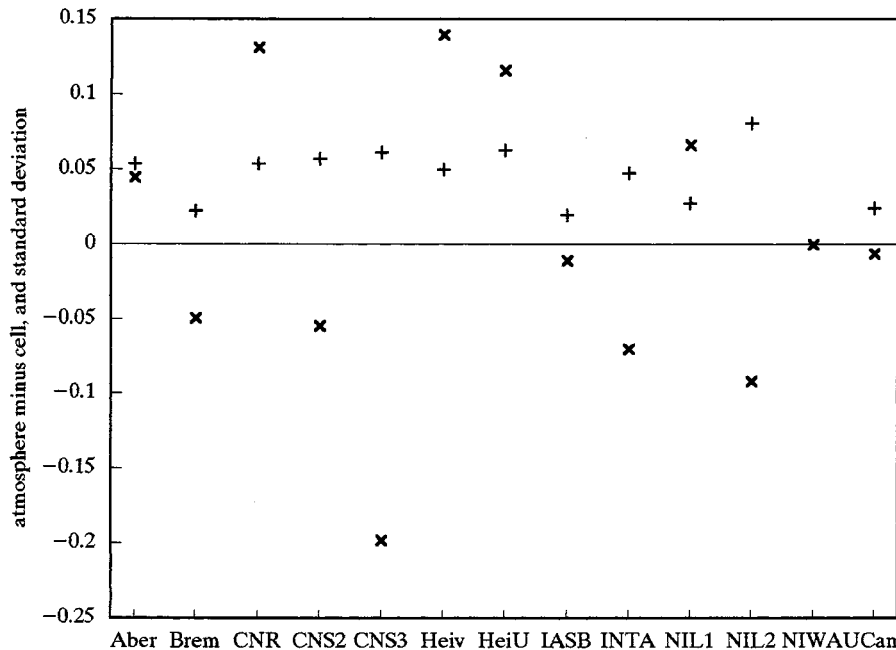


Figure 15. Differences between measurements of the amount in the NO_2 cell and measurements of the slant column of NO_2 in the atmosphere for the whole campaign, after comparison to NIWA values in each case, and after the compensation of the slant column data for cross-sections from Table IX (\times), together with the standard deviations from Figure 12 (+). Note that the difference between cell and atmosphere is not significant at the 2-sigma level for 9 of the instruments, and never exceeds 3-sigma.

tion 3), also smooths the measured spectrum slightly, giving rise to slant columns which are smaller than they should be. The smaller the sampling ratio and the lower-order the interpolation scheme the larger the effect, so this is of particular concern for SAOZ-512 (Aber/CNRS1), which has a small sampling ratio, and uses linear interpolation in the standard software. This may explain why Aber and CNRS1 see 10 to 15% less NO_2 than many instruments in Figure 12. Because the error is zero when the wavelength calibrations of signal and reference are the same, one might expect more noise in the Aber comparison, but the effect may be so non-linear as to change insignificantly at wavelength changes larger than 0.1 pixels, changes which are routinely observed in SAOZ operations. Analysis of a SAOZ-512 spectrum with a cubic spline interpolation gave 15% more NO_2 than a linear interpolation. Future work will evaluate the size and non-linearity of the effect and routinely implement higher-order interpolation.

In one case (INTA) there was evidence that some direct sunlight was being observed by the spectrometer, even at twilight. This would reduce the AMFs and so the slant columns, and probably explains the small values of slant columns of NO_2 for INTA in Figure 12.

Note that except for HeidU, the small differences in wavelength ranges for analysis of NO₂ given in Table V will give rise to differences in AMFs which are far too small to be responsible for the differences in NO₂ discussed here.

7. Conclusions

In this most recent NDSC UV-visible intercomparison, instruments which routinely measure O₃ as well as NO₂ throughout the visible range were compared. Most achieved good accuracy in measurements of O₃. An important exception was the instrument with a wavelength range (408 to 464 nm) which excluded the stronger O₃ features at wavelengths greater than 470 nm, and we conclude that attempting to measure O₃ with a wavelength range specified for NO₂ can lead to poor accuracy. Unlike the earlier UV-visible intercomparison of NO₂ instruments, measurements of NO₂ were analysed using literature cross-sections without a scaling factor: measurements with an NO₂ cell were made as an extra quality check, rather than as a primary calibration.

In our two chosen methods of comparison, we have been careful not to provide plots showing each instrument at each solar zenith angle on each day of the campaign – this would have been an indigestible number of plots. Instead, we have condensed the information into plots of averages, and tables of slopes, residuals and standard deviations.

As previously, regressions of results from instrument pairs over the whole SZA range provided diagnostic information about differences between instruments. Plots of residual errors from the regressions improved the displays of information. Calculations of rms residuals improved our ability to determine the quality of instruments even when slopes of regression analyses were not unity, and provided a powerful new comparison tool when no one instrument was known to be better than others.

Regressions with one of the higher-quality instruments as the comparison show that for O₃ several instruments agree within $\pm 5\%$ of unity in slope. By contrast, for NO₂ only two instruments agree this well, unless all were analysed with the same room-temperature cross-sections over a restricted wavelength range. The latter test was only made with one day's data.

In this intercomparison we also examined fractional differences between instruments averaged over a restricted solar zenith angle range at twilight (85° to 91°), and averaged over the whole campaign. When the higher-quality instruments identified from regressions were used for comparison, the scatter between instruments was similar, independent of which comparison instrument was chosen, and independent of whether single or daily reference spectra were used in analysis. These fractional differences for most instruments fall within $\pm 2.5\%$ (1 sigma) for O₃ and $\pm 6\%$ for NO₂, and are summarised in Table XIII. Although there is clearly still work to do for measurements of NO₂, this is a considerable improvement on the results from the previous intercomparison in U.K. (Vaughan *et al.*, 1997) despite a larger range of instrument styles in this work.

Table XIII. Summary of differences between instruments after removal of three instruments with the largest differences. These are fractional differences of measurements between 85 and 91° SZA. Rms scatter is the standard deviation of each instrument's mean fractional difference, average standard deviation is the average of the standard deviations from each instrument. Each is determined from the scatter of that instrument's fractional difference during all the valid half-days of the campaign

Gas	Cross-section	Reference spectrum	Rms scatter (%)	Average std. dev. (%)
O ₃	Original	Single	2.5	2.1
O ₃	Original	Daily	2.6	1.9
NO ₂	Original	Single	6.0	4.1
NO ₂	Original	Daily	5.2	4.2
NO ₂	Corrected	Single	6.9	4.5
NO ₂	Corrected	Daily	6.9	4.8

Evaluation of standard deviations suggest that the above differences for ozone are barely significant, but for NO₂ they are real differences between instruments. When NO₂ values were corrected by the correlation coefficient between each instrument's preferred cross-sections and a common set of low-temperature cross-sections, the pattern of disagreement changed but the mean scatter between instruments did not decrease.

The ratio of NO₂ found using room-temperature cross-sections to NO₂ found using low-temperature cross-sections depends on the exact details of wavelength range and spectral resolution. There are now several published sets of low temperature NO₂ cross-sections. We suggest that NDSC and other interested organisations (AFGL, ESA, NASA) agree on a recommended set of low-temperature cross-sections, and that all analyses use this recommended set, as well as any other chosen set if desired.

Measurements with an NO₂ cell also showed a similar scatter between instruments, but with a different pattern, even after compensating for the small temperature coefficient of NO₂ in the cell. Some differences in pattern between cell and atmosphere were just significant at the 2-sigma level. Hence cell measurements introduced a similar degree of error to that of the atmospheric intercomparison.

We conclude that zenith-sky UV-visible instruments which observe the stronger features of O₃ at wavelengths longer than 470 nm for measurements of O₃ are in good agreement, despite differing sources of cross-sections; but that instruments which measure NO₂ have significant disagreements. There are several possible

sources of disagreements in NO₂ amounts within the instruments, the analysis procedures and the cross-sections, and these will be investigated in detail in future work.

Acknowledgements

We wish to thank the staff at OHP, particularly those at the Lidar building who put up with extreme disruption to their office, work and coffee facilities with good humour, and who provided us with lasers with which to test the stray-light performance of several of the spectrometers. We thank the staff at the residence for their excellent food, which also helped guarantee that much more work was done because we had no wish to leave the site each evening. The project and most authors were supported by EU Contract ENV4-CT95-0089 (SCUVS-3). I. Kostadinov was supported by the ICTP Programme for Training and Research in Italian Laboratories, Trieste.

References

- Alliwell, S. R. and Jones, R. L., 1996: Measurement of atmospheric NO₃. 1. Improved removal of water vapour absorption features in the analysis for NO₃, *Geophys. Res. Lett.* **23**, 2585–2588.
- Anderson, S. M. and Mauersberger, K., 1986: Laser measurements of ozone absorption cross-sections in the Chappuis band, *Geophys. Res. Lett.* **13**, 1,256–1,259.
- Bass, A. M. and Pauer, R. J., 1985: The ultraviolet cross-sections of ozone. I. Measurements, in C. S. Zerofos and A. Ghazi (eds), *Proc. Quadrennial Ozone Symp. Halkidiki, Greece, 3–7 Sept. 1984*, Reidel, Dordrecht, pp. 606–616.
- Brewer, A. W., McElroy, C. T., and Kerr, J. B., 1973: Nitrogen dioxide concentrations in the atmosphere, *Nature* **246**, 129–133.
- Brion, J., Chakir, A., Daumont, D., Malicet, J., and Parisse, C., 1993: High resolution laboratory absorption cross-sections of O₃, temperature effect, *Chem. Phys. Lett.* **213**, 610–612.
- Burrows, J. P., Dehn, A., Deters, B., Himmelmann, S., Richter, A., Voigt, S., and Orphal, J., 1998: Atmospheric remote sensing reference data from GOME: Part 1. Temperature dependent absorption cross-sections of NO₂ in the 231–794 nm range, *J. Quant. Spectrosc. Radiat. Transfer*, in press.
- Coquart, B., Jenouvrier, A., and Merienne, M. F., 1995: The NO₂ absorption spectrum. II. Absorption cross-sections at low temperature in the 400–500 nm region, *J. Atmos. Chem.* **21**, 251–261.
- Erle, F., Pfeilsticker, K., and Platt, U., 1995: On the influences of tropospheric clouds on zenith-scattered-light measurements of stratospheric species, *Geophys. Res. Lett.* **22**, 2725–2728.
- Fish, D. J. and Jones, R. L., 1995: Rotational Raman scattering and the Ring effect in zenith-sky spectra, *Geophys. Res. Lett.* **22**, 811–814.
- Greenblatt, G. D., Orlando, J. J., Burkholder, J. B., and Ravishankara, A. R., 1994: Absorption measurements of oxygen between 330 and 1140 nm, *J. Geophys. Res.* **95**, 18,577–18,582.
- Gil, M., Puentedura, O., Yela, M., Parrondo, C., Thorkelsson, B., and Jadhav, D., 1996: OCIO, NO₂ and O₃ total column observations over Iceland during the winter 1993/94, *Geophys. Res. Lett.* **23**, 3320–3323.
- Giovanelli, G., Bonasoni, P., Cervino, M., Evangelisti, F., and Ravegnani, F., 1994: Ozone ground-based measurements by the GASCOD near-UV and visible DOAS system, *Proc. Quadrennial Ozone Symp. 1992, Ozone in the troposphere and stratosphere* (ed. R. D. Hudson), NASA Conference Publication 3266, Washington D.C., pp. 707–711.
- Hald, A., 1952: *Statistical Theory with Engineering Applications*, Wiley, New York, p. 537.

- Harder, J. W., Brault, J. W., Johnston, P. V., and Mount, G. H., 1997: Temperature dependent NO₂ cross-sections at high spectral resolution, *J. Geophys. Res.* **102**, 3,862–3,879.
- Harwood, M. H. and Jones, R. L., 1994: Temperature dependent ultraviolet-visible absorption cross-sections of NO₂ and N₂O₄: Low temperature measurements of the equilibrium constant for 2 NO₂ ⇌ N₂O₄, *J. Geophys. Res.* **99**, 22,955–22,964.
- Hofmann, D. J. *et al.*, 1995: Intercomparison of UV/visible spectrometers for measurements of stratospheric NO₂ for the network for the detection of stratospheric change, *J. Geophys. Res.* **100**, 16,765–16,791.
- Karlsen, K., Floisand, I., Kastad Hoiskar, B. A., and Braathen, G., 1996: Ground-based measurements of O₃, NO₂, OClO and BrO with a new UV-vis spectrometer at NyAlesund, Spitsbergen in winter 95/96, published abstract 262 at Quadrennial Ozone Symposium, September 1996, L'Aquila.
- Kerr, J. B., McElroy, C. T., Wardle, D. I., Olafson, R. A., and Evans, W. F. J., 1985: The automated Brewer spectrophotometer, in C. S. Zerefos and A. Ghazi (eds), *Atmospheric Ozone, Proc. Quad. Ozone Symp., Greece, 3–7 Sept. 1984*, Reidel, Dordrecht, pp. 543–546.
- Merienne, M. F., Jenouvrier, A., and Coquart, B., 1995: The NO₂ absorption spectrum. I. Absorption cross-sections at ambient temperature in the 300–500 nm region, *J. Atmos. Chem.* **20**, 281–297.
- Noxon, J. F., 1975: Nitrogen dioxide in the stratosphere and troposphere measured by ground-based absorption spectroscopy, *Science* **189**, 547–549.
- Otten, C., Ferlemann, F., Platt, U., Wagner, T., and Pfeilsticker, K., 1998: Ground-based DOAS UV/visible measurements at Kiruna (Sweden) during the SESAME winters 1993/94 and 1994/95, *J. Atmos. Chem.*, in press.
- Pommereau, J-P. and Goutail, F., 1988: Stratospheric O₃ and NO₂ observations at the southern polar circle in summer and fall 1988, *Geophys. Res. Lett.* **15**, 895–897.
- Preston, K. E., Roscoe, H. K., and Jones, R. L., 1997: Retrieval of NO₂ vertical profiles from ground-based UV-visible measurements: Method and validation, *J. Geophys. Res.* **102**, 19,089–19,097.
- Richter, A., 1997: Spectroscopic measurements of stratospheric absorbers above Bremen, 53° N, PhD thesis, University of Bremen.
- Roscoe, H. K., Fish, D. J., and Jones, R. L., 1996: Interpolation errors in UV-visible spectroscopy for stratospheric sensing: Implications for sensitivity, spectral resolution and spectral range, *Applied Optics* **35**, 427–432.
- Roscoe, H. K. and Hind, A. K., 1993: The equilibrium constant of NO₂ with N₂O₄ and the temperature dependence of the visible spectrum of NO₂: A critical review and the implications for measurements of NO₂ in the polar stratosphere, *J. Atmos. Chem.* **16**, 257–276.
- Roscoe, H. K. and Wells, R. J., 1989: The variation of pressure, temperature and transmission within a pressure modulator: Measurements with a high-compression modulator, *J. Quant. Spectrosc. Radiat. Transfer* **41**, 259–285.
- Rothman, L. S. *et al.*, 1992: The HITRAN molecular database – Editions of 1991 and 1992, *J. Quant. Spectrosc. Radiat. Transfer* **48**, 469.
- Sarkissian, A., Roscoe, H. K., Bartlett, L. M., Vaughan, G., O'Connor, F., Hughes, P., Moore, D., and Drew, D., 1997: Accuracy of measurements of total ozone by a SAOZ ground-based spectrometer, *J. Geophys. Res.* **102**, 1,379–1,390.
- Vaughan, G. *et al.*, 1997: An intercomparison of ground-based UV-visible sensors of ozone and NO₂, *J. Geophys. Res.* **102**, 1,411–1,422.
- Van Daele, A. C., Hermans, C., Simon, P. C., Van Roozendaal, M., Guilmot, J. M., Carleer, M., and Colin, R., 1996: Fourier transform measurement of NO₂ absorption cross-section in the visible range at room temperature, *J. Atmos. Chem.* **25**, 289–305.
- Vosper, A. J., 1970: Dissociation of dinitrogen tetroxide in the gas phase, *J. Chem. Soc.* **A325**, 625–627.